TOTAL RADIATION AND ELECTRICAL ARC CHARACTERISTICS OF AN AIR PLASMA

A THESIS

Presented to

The Faculty of the Division of Graduate

Studies and Research

By

Johnny G. Cailleteau

In Partial Fulfillment

of the Requirements for the Degree

Master of Science in Mechanical Engineering

Georgia Institute of Technology

August, 1974

TOTAL RADIATION AND ELECTRICAL ARC
CHARACTERISTICS OF AN AIR PLASMA

Approved:

W. Z. Black, Chairman

P. Durbetaki

J. R. Williams

E. W. Thomas

Date approved by Chairman: 10/17/74

ACKNOWLEDGMENTS

I wish to express my sincere appreciation to the members of my reading committee, Drs. W. Z. Black, P. Durbetaki, J. R. Williams, and E. W. Thomas, for their valuable suggestions and help in preparing the final draft. I would also like to thank Drs. R. S. Devoto and U. H. Bauder for suggesting the topic of this thesis. I am indebted to them for their guidance and encouragement throughout the research.

Finally, I wish to acknowledge the support of Arnold Engineering Development Center at Tullahoma, Tennessee, in connection with this research project.

TABLE OF CONTENTS

Page

ACKNOWLEDGMENTS. ii

LIST OF TABLES iv

LIST OF ILLUSTRATIONS. v

NOMENCLATURE vi

SUMMARY. viii

Chapter

I. INTRODUCTION. 1

II. THEORY OF RADIATION TRANSPORT 4

III. APPARATUS 10

IV. PROCEDURE 19

V. FIELD STRENGTH RESULTS. 23

VI. POWER RADIATED PER UNIT ARC LENGTH FOR AIR. . . . 27

VII. TOTAL RADIATION AS MEASURED FOR AIR 34

VIII. CONCLUSIONS 43

APPENDIX

A. CALCULATION OF TRANSMITTANCE. 46

B. CALCULATION OF THE APPARENT LENGTH. 48

C. SOLID ANGLE CALCULATIONS. 54

D. SAMPLE CALCULATIONS FOR U(T). 57

REFERENCES 59

LIST OF TABLES

Table Page

1. List of Instruments. 16

LIST OF ILLUSTRATIONS

Figure		Page
1.	Schematic Diagram of Gas Feed System.	11
2.	Schematic Diagram of Experimental Apparatus	13
3.	Electric Field Strength of Air as a Function of Arc Current	24
4.	Electric Field Strength of Air Compared to Nitrogen.	26
5.	Power Radiated Per Unit Arc Length for Air.	30
6.	Power Radiated from Air and Nitrogen as a Function of Arc Current	32
7.	Power Radiated from Air and Nitrogen as a Function of Power in	33
8.	Radial Temperature Profiles Used for Calculating U(T).	37
9.	Radial Temperature Profiles Used for Calculating U(T).	38
10.	Temperature Versus Normalized Radius.	39
11.	Total Radiation as Measured for Air	41
12.	Total Radiation for Air and Nitrogen.	42
13.	Schematic Diagram of Shaded and Unshaded Areas.	49
14.	Angles Intercepted by Thermopile.	50
15.	Solid Angle Intercepted by Thermopile	55

NOMENCLATURE

ε_λ	emission coefficient for a specified wavelength
e	elementary charge
n_e	particle density of the electrons
k	Boltzmann constant
m	mass of the electron
λ	wavelength
T	temperature
γ	statistical weight of the parent ion
Z_1	partition function of the ion
h	Planck constant
c	speed of light
ξ^{fb}	free-bound factor
ξ^{ff}	free-free factor
A_n^m	Einstein transition probability
n_a	particle density of atoms
g_m	statistical weight of the upper level
Z_a	partition function of atoms
E_m	excitation energy of the level m
T_R	thermopile reading
P_R	power radiated
ω	solid angle
ℓ'	apparent length of the arc
τ	transmittance of quartz windows

A_2	area of thermopile
S	distance between arc and thermopile
T_a	axis temperature of the arc
T_w	wall temperature
R	radius of the arc channel
U	total volumetric radiation coefficient
ρ	normalized radius
B	slope of the total radiation curve between successive axis temperatures
ϕ	ratio of reflected light to incident light
n	index of refraction
Z_{us}	area in the unshaded region
Z_s	area in the shaded region

SUMMARY

This thesis was concerned with the determination of the electrical arc characteristic and the total radiation of an air plasma at atmospheric pressure. The plasma was generated by a dc electric cascade arc.

Observation of the arc column was achieved by the use of a side-on viewing port made of fused quartz. Measurement of the radiation emitted by the air plasma through this port was accomplished by the use of a thermopile placed at a measured distance from the arc column. These thermopile readings were converted to the power radiated per unit arc length emitted by the plasma and were used in the determination of the total radiation. The total radiation was determined by solving the Volterra integral equation using a numerical step-by-step procedure. The result of this calculation was the total radiation as a function of temperature. These results when compared with the total radiation emitted by nitrogen arcs, showed that the total radiation calculated in this study was consistently higher than the total radiation from nitrogen.

The electrical arc characteristic was obtained by converting plots of voltage on the cascade plates as a function of axial distance in the cascade to field strengths for various currents. These field strength measurements

agreed closely with those obtained in nitrogen.

Results of total radiation and electrical field strength obtained in this study indicate that the dc electric cascade arc can be used as a device for determining transport properties of gases. Protection of the electrodes from oxidation by the air also demonstrated that a gas can be introduced into the arc column at low flow rates without creating any detectable convection effects.

CHAPTER I

INTRODUCTION

The properties of air at high temperatures, and pressures of one atmosphere and above have become increasingly important in engineering applications. Some examples of these applications are re-entry of hypersonic vehicles, transport properties of gases in the vicinity of intense explosions, wind-tunnel arc heaters, arc light sources, and high-current circuit breakers. Forecasting of flow fields and characteristics for these applications requires a knowledge of the thermodynamic and transport properties of air. Although there are many difficulties associated with calculations of properties in air, there have been accurate calculations made of the thermodynamic properties of air.

A knowledge of the transport properties of air, however, is not nearly so widespread. Yos [1] has calculated these properties, but the results have not been verified experimentally. This lack of experimental data is due largely to the difficulties encountered in heating the air to high temperatures.

This research project, initiated by a contract from Arnold Engineering Development Center at Tullahoma, Tennessee, was motivated primarily due to the scarcity of experimental

work in air plasmas. The purpose of this project was to determine the transport properties of air, namely: the thermal conductivity, k(T); electrical conductivity, $\sigma(T)$; and the total radiation, U(T).

This thesis deals specifically with the electrical arc characteristics and the total radiative power for an air plasma at a pressure of one atmosphere. Ultimately, these results, together with the temperature profiles determined by Shires [5], will be used by other researchers to calculate the electrical and thermal conductivities for air at one atmosphere.

The device used to deduce these properties was the wall-stabilized electric arc. This apparatus, first developed in Germany by Maecker, has been used in argon, hydrogen, and nitrogen by H. Maecker, U. Bauder, and associates [2] to measure electrical conductivity, thermal conductivity, and radiative properties over a large pressure and temperature range.

In order to determine the electrical and thermal conductivity, there are several quantities which must first be measured. In the case of the electrical conductivity, the field strength and the radial temperature profiles in the gas must be known for various arc currents. For the deduction of the thermal conductivity, however, the above data plus information on radiative losses is required, if conduction is the dominant heat transfer mode within the gas.

Recent work has been published by Schreiber, Hunter, and Benedetto [3] on the temperature profiles, electrical conductivity, and radiative losses in an air plasma. This work was conducted using a flowing, pulsed electric arc discharge with a maximum pulse duration of one second and a channel diameter of one inch. Oxidation of the electrodes was prevented by a nitrogen atmosphere which was allowed to flow through the test section. The major differences in the arc facility used in this research as compared to that of reference 3 are: (1) continuous as opposed to pulsed operation, (2) smaller channel diameter, (3) argon protector shield, and (4) no flow through the test section.

The only other known experimental research in air was conducted by E. I. Asinovsky, A. V. Kirillin, E. P. Pakhomov, and V. I. Shabashov [4]. These experiments, carried out at the USSR Academy of Sciences, were performed using a wall-stabilized dc-arc, 100-200 mm in length. The electrodes were protected from oxidation by an argon blanket.

CHAPTER II

THEORY OF RADIATION TRANSPORT

Determination of the radiation emitted from the air plasma at one atmosphere pressure was performed on the basis of the following assumptions: (1) existence of local thermodynamic equilibrium (LTE) in the plasma, (2) optically thin plasma to radiation from visible lines and continuum, (3) steady-state operation, and (4) no axial gradients (i.e., cylindrical symmetry) in the test section.

The assumptions of no axial gradients in the test section and steady-state operation were justified in the following manner. The absence of axial gradients in the test section was demonstrated by a constant field strength in this region. Cylindrical symmetry has been used in the investigation of nitrogen by Hermann and Schade [6] and by a number of other researchers [2,6,7]. A photocell was used to detect steady-state operation of the arc column. The photocell output, displayed on an oscilloscope, provided a means of continuously monitoring the stability of the arc.

Assumptions of local thermodynamic equilibrium have been used by a number of researchers for operations of cylindrical arcs in nitrogen [6,7] and air at one atmosphere [3]. This assumption allows temperature distributions to

be determined from spectrometric measurements of the intensity of line or band radiation if the appropriate transition probabilities are known.

An optically thin plasma is one in which the radiation emitted is not absorbed within the arc column but escapes to the cascade walls. It has been determined [9] that an air plasma is optically thin to continuum radiation at one atmosphere for wavelengths greater than 114 nm. Since radiation from lines is also important, an investigation of about 200 NI and OI lines [9] reveals that the plasma, for $\lambda \geq 200$ nm, is optically thin to radiation for plasmas at one atmosphere. For a number of lines in the vacuum ultraviolet ($\lambda < 200$ nm) the plasma is optically thick to radiation. However, due to the properties of the quartz windows used in the experiments, radiation below 200 nm was not received. Therefore the assumption of an optically thin plasma holds for the region investigated.

Radiation from hot air is due to three mechanisms: (1) molecular radiation, (2) continuum radiation, and (3) atomic line radiation. For temperatures up to 8000°K, the dominant radiation source is from the molecular bands of N_2 and N_2^+. At this temperature radiation is small in comparison to conduction and hence plays a negligible role in the energy transport. At temperatures above 8000°K atomic line radiation and continuum radiation become the dominant source of radiant energy.

Continuum radiation occurs in transitions where the electron can occupy a continuum of energy levels, and is composed of two parts [10]: (1) free-bound (i.e. $e^- + N^+ = N +$ photon) and (2) free-free electronic transitions (i.e. $e^- + N^+ = e^- + N^+ +$ photon). Free-bound transitions are exemplified by radiative recombination, that is, the capture of a free electron by an ion. The second portion, free-free transitions, refers to the interaction of a free electron with an ion in which the electron is decelerated but not captured, with the change in kinetic energy of the electron appearing as radiation. Utilizing these exchange mechanisms and assuming thermal equilibrium [8,11] the emission coefficient for a specified wavelength, ε_λ, may be written as:

$$\varepsilon_\lambda = \frac{8\sqrt{2\pi}\, e^6}{3\sqrt{3km^3}\, c^2} \frac{n_e^2}{\lambda^2\sqrt{T}} \xi(\lambda,T) \qquad (2\text{-}1)$$

where:

$$\xi(\lambda,T) = \frac{\gamma}{Z_1} \xi^{fb}(\lambda,T)\left[1-\exp\left(\frac{-hc}{\lambda kT}\right)\right] + \xi^{ff}(\lambda,T)\exp\left(\frac{-hc}{\lambda kT}\right)$$

γ = statistical weight of the parent ion

k = Boltzmann constant

λ = wavelength

Z_1 = partition function of the ion

h = Planck constant

c = speed of light

T = temperature

e = elementary charge

ε_λ = continuous emission coefficient

m = mass of the electron

n_e = particle density of the electrons

ξ^{fb} and ξ^{ff} represent the free-bound and free-free factors. In air the continuum radiation is due mostly to the free-bound transitions as in the case of $e^- + N^+$ and $e^- + O^+$. It is also due to minor recombinations such as $e^- + NO^+$, $e^- + N_2^+$, etc. This emission coefficient, ε_λ, can be integrated over all wavelengths, i.e. $\int_o^\infty \varepsilon_\lambda d\lambda$, to give the total continuum emission coefficient, U_c. In the present experiment, however, quartz windows limited radiation measured to that emitted between λ = 200 nm and λ = 4000 nm.

Line radiation, on the other hand, occurs in transitions between clearly defined energy levels. This type of radiation is composed of bound-bound radiative electronic transitions. These transitions are characterized by shifts from an excited electronic state to a lower electronic state. Line radiation, U_L, can be calculated by summing the emission coefficient, ε_L, over the atomic lines. This emission coefficient (for atomic lines only) is given by U. Bauder [11] as:

$$\varepsilon_L = \frac{h_c}{4\pi\ \lambda_{mn}} \frac{A_n^m\ n_a\ g_m}{Z_a} e^{-\frac{E_m}{kT}} \qquad (2\text{-}2)$$

where

A_n^m = Einstein transition probability

n_a = particle density of atoms

g_m = statistical weight of the upper level

Z_a = partition function of atoms

E_m = excitation energy of the level m

k = Boltzmann constant

h = Planck constant

T = temperature

λ_{mn} = wavelength of the line

c = speed of light

This equation is valid for each line of each atom and can be summed over the atomic lines to yield the total line radiation, U_L, which can be written as:

$$U_L = \sum_{\text{atomic lines}} \varepsilon_L \qquad (2\text{-}3)$$

Sensitivity to atomic line radiation was reduced by the quartz windows and, as in the case of the continuum radiation, only radiation within the wavelength range of λ = 200 nm to λ = 4000 nm was measured.

Since both lines and continuum contributed to the total radiation emitted, it is important to note that within

the wavelength range of the measured radiation, 200 nm $\leq$ $\lambda \leq$ 4000 nm), previous research in air plasmas [3] has determined that line and continuum radiation is equally important for temperatures between 9000°K and 12400°K. However, if radiation from the vacuum ultraviolet (λ < 200 nm) is taken into account, as done by Hermann and Schade [6], then radiation from atomic lines is dominant at about 10,000°K.

CHAPTER III

APPARATUS

A wall-stabilized or cascade arc, first described and revised by Maecker and coworkers [19] and later used at high pressures by Bauder and Stephens [13], was used. This particular arc provided cylindrical symmetry of the arc column and a knowledge of the boundary conditions necessary for the determination of the transport properties. The basic components of this system consisted of: (1) a pressure vessel containing the arc electrodes and copper plates, (2) a gas feed system, and (3) a water coolant system which supplied the necessary cooling for those parts of the apparatus in direct contact with the plasma. This apparatus permitted continuous operation as opposed to the pulsed-type of operation [3].

The pressure vessel had an inner diameter of 20 cm and was constructed of 4340 steel. The arc channel was composed of 16 individually water-cooled cascade plates, 2 mm thick and having a central bore of 5 mm (Figure 1). These plates were electrically insulated from each other by .3 mm thick silicone rubber washers. The electrode system was composed of a tapered tungsten cathode 5 mm in diameter positioned on the axis of the system; the anode was constructed

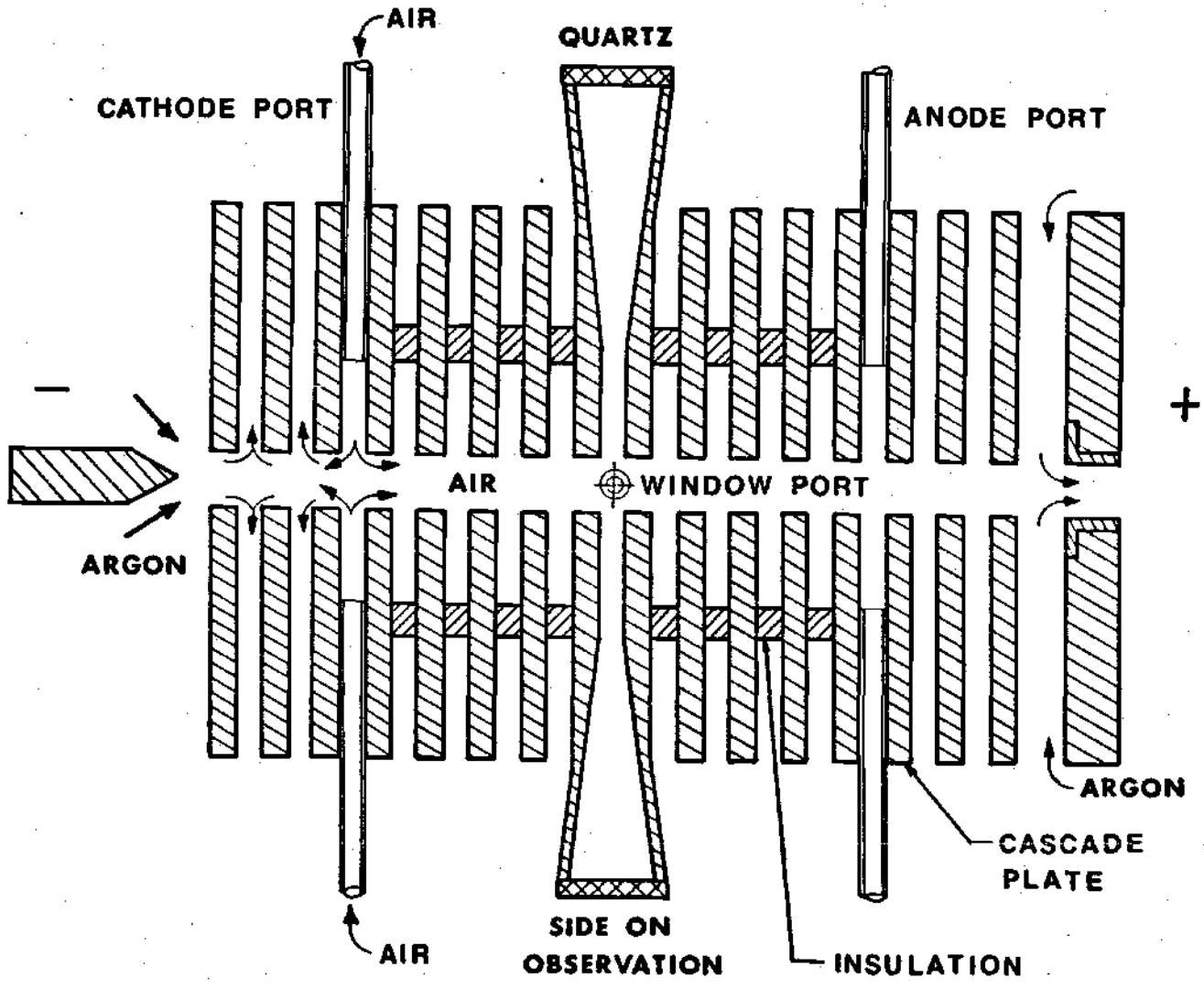

Figure 1. Schematic Diagram of Gas Feed System

by modifying a copper cascade plate 5 mm thick.

Side-on observation of the arc was accomplished by two sets of quartz windows (Figure 2). The two ports permitted both spectroscopic and total radiation measurements.

The gas feed system, shown schematically in Figure 1, was designed to allow operation with air. The electrodes were surrounded with a blanket of argon to protect them against oxidation by the test gas. Introduction of air into the test section was provided for by the use of graduated needle valves and entrance ports placed at the cathode, window, and anode. The amount of gas introduced into each port was regulated individually with the central supply being a single bottle of compressed air. A pressure sensing diaphragm was used to measure the pressure in the air supply line.

Circulation of the cooling water through the cascade plates and electrodes was provided for by means of a Petrodyne dual pump, which maintained a constant water flow of approximately 40 liters/minute at a static pressure equal to that of the gas in the chamber. Heat was transferred from the cooling water after flowing through the arc apparatus by means of a 300 kw heat exchanger before returning to the pump.

Distilled water was used as the coolant owing to the high resistivity required for experiments with cascade arc discharges. In order to maintain as high a purity as

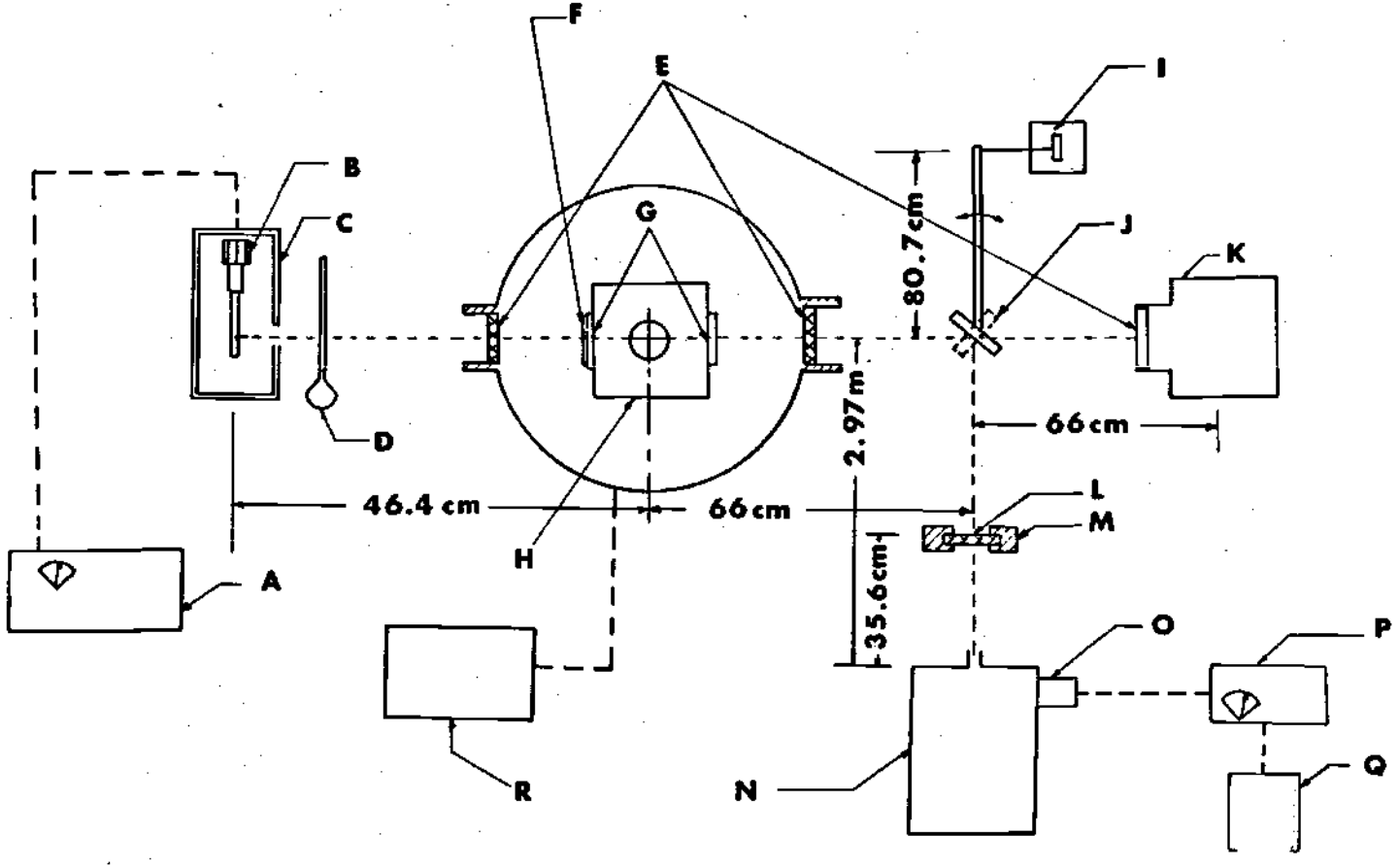

Figure 2. Schematic Diagram of Experimental Apparatus

Description of Figure 2

A. Nanovoltmeter

B. Thermopile

C. Thermopile Housing

D. Protective Shutter

E. Quartz Windows (outer)

F. Razor Blade Slit

G. Quartz Windows (inner)

H. Cascade Plates

I. Motor and Reducer

J. Mirror

K. Standard Lamp

L. Lens

M. Limiting Aperature

N. Spectograph and Monochromator

O. Photomultiplier

P. Picoammeter

Q. Strip Chart Recorder

R. X-Y Recorder

possible, a system consisting of two filtering units was used as a water purification device.

Measurement of the total radiation was achieved with the apparatus shown schematically in Figure 2, consisting of parts A, B, C, and D. A Hilger-Schwarz thermopile, B, Model FT.19/463 (Table 1) was placed at a measured distance from the side-on quartz observation window E. A protective shutter, D, was provided to prevent excessive overheating due to incident radiation. The thermopile was mounted on a motor-driven stand to allow scans in the vertical direction for determining the maximum amplitude of the radiation. In order to simplify the analysis of the solid angle, a .25 mm x 5 mm razor blade slit, shown in Figure 2 as part F, was used to limit the amount of light intercepted by the thermopile. A Keithley nanovoltmeter, Model 148, was connected to measure the output of the thermopile. Cancellation of effects from radiation of the surrounding atmosphere was achieved by use of a zero-suppression circuit available on the nanovoltmeter.

Data for determination of the electrical arc characteristics were collected by using the cascade plates as probes and a motor-driven stepper to measure the voltage between the anode and the cascade plates. Outputs were displayed in analog form on a Hewlett-Packard X-Y recorder, Model 7004A.

Radial temperature profiles were determined from

Table 1. List of Instruments

A.	Nanovoltmeter:	Keithley Instruments, Inc. Model 148 Battery or A-C Operation Accuracy = 1% of full scale
B.	Thermopile:	Hilger-Schwarz Type FT 19/463 Receiver Dimensions: 2 x .2 mm Sensitivity: 25 μV/μW Response Time: .01 sec Spectral Range: 110-10000 nm
C.	Thermopile Housing	
D.	Protective Shutter	
E.	Quartz Windows (outer)	2.5 cm thick 3.8 cm dia Limiting Aperature = 2.54 cm Index of Refraction ≈ 1.52
F.	Razor Blade Slit:	.25 x 2 mm
G.	Quartz Windows (inner)	5 x 3 x 4 mm
H.	Cascade Plates	2 x 25.15 mm each
I.	Motor and Reducer:	Globe Industries A-C Motor 20 rpm Gaertner Scientific Corporation Reducer and slide.
J.	Mirror:	12.7 x 8.8 cm Pivoted in the center
K.	Standard Lamp:	EG & G Model 590 Calibrated Lamp System 5920 Lamp Housing Calibrated by Epply Laboratories, Inc. Spectral Range of Calibration 250 nm to 750 nm National Bureau of Standards Reference Standards Employed: EU 285, EU 286, EU289

Table 1 (concluded)

L. Lens: Karl Lambrecht
Crystal-Quartz-Lithium Floride Achromatic
Objective Lens
Diameter = 32 mm
Focal Length 80 ± 5 cm
Chromatic Error of .5% or less
Throughout spectral Range λ = 210 nm to λ = 600 nm

M. Limiting Aperature: 38 mm outside diameter
29 mm clear

N. Spectrograph & Monochromator: McPherson

O. Photomultiplier: EMI 6255S

P. Picoammeter: Keithley Instruments
Model 416
High speed
Response Time ≈ .004 sec

Q. Strip Chart Recorder: Clevite Brush
Mark 250 Recorder

R. X-Y Recorder: Hewlett-Packard
Model 7004A

side-on measurements with a McPherson spectograph and monochromator. Outputs from a Keithley picoammeter in conjunction with an EMI photomultiplier tube were recorded on a Clevite Brush strip chart recorder. These outputs, or lateral intensity profiles, were converted to radial emission coefficients by use of the Abel inversion computer program developed at Wright Patterson Air Force Base. Calibration was achieved by using a Model 590, EG & G, standard lamp, calibrated to the National Bureau of Standard's reference. These measurements are described in detail by Shires [5].

CHAPTER IV

PROCEDURE

The cascade was first filled entirely with argon gas before the arc discharge was started. This precaution was taken so that there was no danger of air being present in large quantities in the chamber and causing oxidation of the electrodes. Next, air was allowed to enter through the cathode port.

The purity of the air was determined spectroscopically by scanning the spectrum in the vicinity of the strong argon lines at 425.9, 426.6, 427.2, 430.0 and 433.3 nm. Disappearance of these lines was used as justification of the purity of the air present in the test section.

Possible contamination of the test section by vapors from the tungsten electrode was also investigated. The absence of tungsten was determined, again, by spectroscopic measurements. Spectral scans were made with the air arc in operation at a current of 80 amps. These scans were made at wavelengths of 429.4 nm and 430.2 nm, which are strong tungsten lines. Results of this investigation showed that these lines, and therefore tungsten, was not present in any discernable amounts.

Another test was conducted to determine whether the

convective mode of energy transport caused by the motion of the gas introduced into the test section (cathode port) had a significant effect on the measurements. In this test the chamber was filled with nitrogen and field strengths and lateral intensity profiles were recorded. Next, the chamber was filled completely with argon, and nitrogen was introduced into the port at the same flow rate used for air. Again field strengths and lateral profiles were measured. Comparison of these two measurements revealed that they were in agreement within approximately 3%. These measurements justified the absence of convective effects in the test section, thus allowing the determination of the thermal conductivity by considering only radiative transfer of energy.

Optical alignment of the system, shown schematically in Figure 2, was accomplished by use of a small laser. The method for aligning the system was as follows. First, the spectograph was set at zero wavelength. Then the laser beam was focused into the spectograph such that light was reflected from the mirrors inside and out through a pinhole positioned on the entrance slit. Next, the light exiting from the spectograph was directed into the quartz windows on the cascade, and the chamber was adjusted until the intensity of light emerging from the opposite viewing port was a maximum. This alignment was performed without the lens to avoid having it correct what would otherwise be a poor alignment. The lens was mounted on a stand and adjusted to

complete the alignment. The thermopile was also placed in line with the laser beam. This was achieved by adjusting a horizontal carriage on the thermopile support until the laser light exiting from the cascade was incident directly on the element. This procedure assured that the thermopile was aligned correctly in the horizontal position. A scanning motor was provided so that vertical alignment could be attained by remote control, except for the last few times when this motor failed.

Radiation data were collected at the following arc currents: 28, 31, 35, 40, 42, 60, 70, 80, 90, 100, 120, and 140 amps, using the following procedure. Once the arc was started and air introduced into the test section, the scale on the nanovoltmeter was set at zero by using the built-in zero suppression circuit. This step, in effect, eliminated interference from radiation due to the surrounding atmosphere. The shutter was lowered and the thermopile was scanned vertically by remote control to obtain a maximum reading. This value was recorded and then rechecked several times during the air operation to reduce the possibility of an error.

Field-strength data was collected for all of the above currents and also for following currents: 12, 19, 54, and 160 amps. The actual data collected resulted in a plot of the voltage on the plates. These data were used to determine the field strengths as described in the next section. The

device for stepping the voltage sensor was operated by remote control from the main panel. Currents were measured using a precision shunt resistor.

These data were reduced to determine the power radiated per unit length, the total radiation per unit volume, and the electrical arc characteristic which are presented and discussed in Chapters V, VI, and VII.

CHAPTER V

FIELD STRENGTH RESULTS

The determination of the electrical arc characteristic took place in the following manner. First, the data for the voltage between plates as a function of axial distance through the cascade were used to provide an average voltage-distance curve. Due to the absence of axial gradients these plots were straight lines. Next, the voltage difference between cascade plates 6 and 12 was divided by the distance separating these plates (≈1.43 cm), thus yielding the field strength in volts/cm. This method was used for all of the measurements taken, from arc currents as low as 12 amperes to values of current as high as 160 amperes. The results were plotted as a function of arc current and are shown in Figure 3.

This plot illustrates the typical high field strength at low current. The minimum field strength occurs at about 80 amperes. The flattening of the curve at higher currents is probably due to the increasing importance of radiation [21]. A smooth curve was drawn through these data points in order to give other researchers a smooth, continuous function to work with in determining the electrical conductivity.

An error band of approximately 5% was expected in the voltage measurements. This was due to leakage or bypass

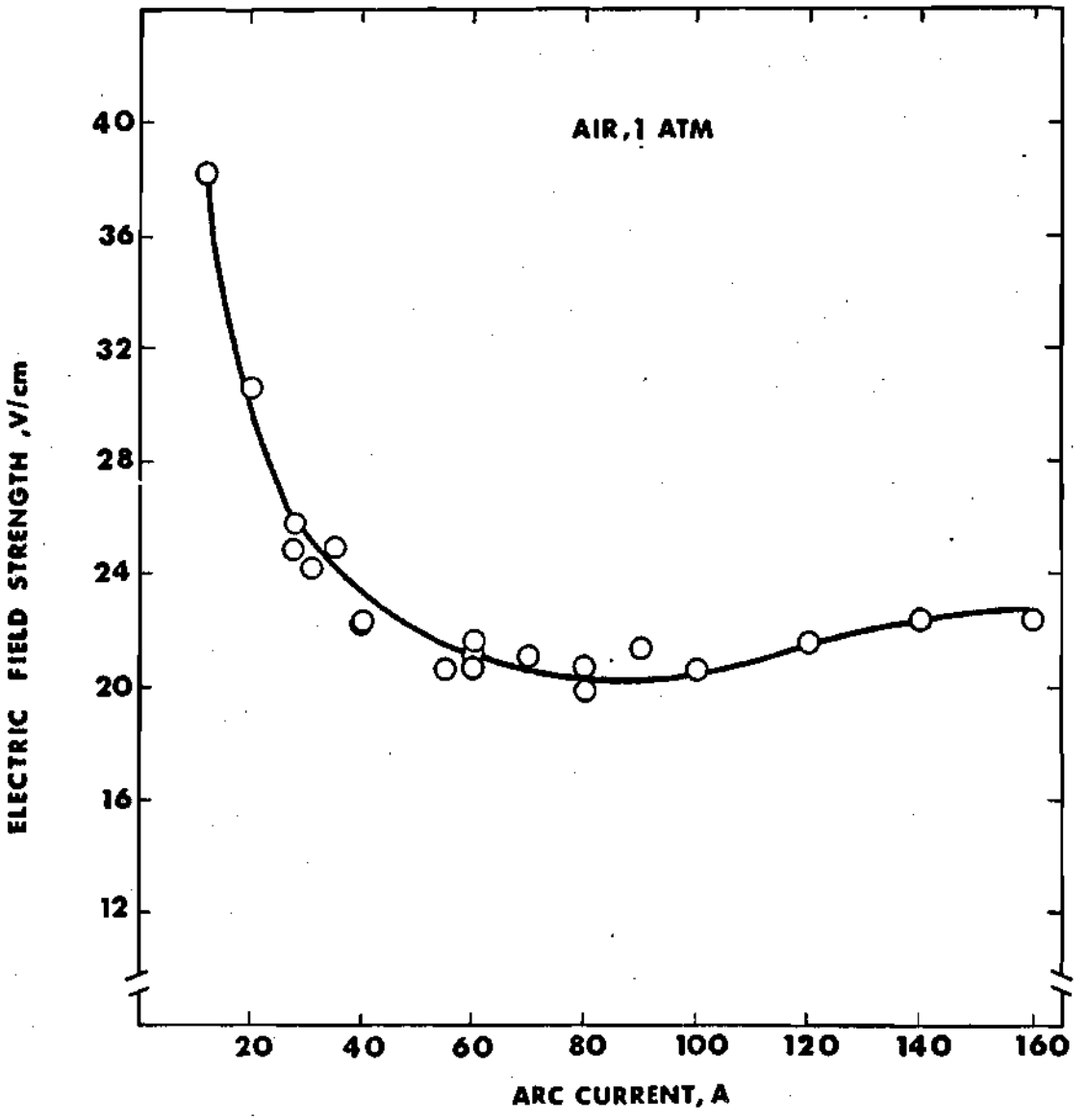

Figure 3. Electric Field Strength of Air as a Function of Arc Current

current flowing between cascade plates through the cooling water. This error in measurement is evidenced in the figure by the scattering of points about the curve. All of the calculated points lie within 5% of the values of the smoothed curve.

Figure 4 is a comparison between the arc characteristic, as measured for air, and the characteristic of nitrogen as measured by Maecker and coworkers [14]. As illustrated by this figure, the two results are in close agreement, probably due to the large quantity of nitrogen present in air.

As stated in the introduction, the electrical conductivity may be determined for air using these results and the radial temperature profiles. Methods for performing these calculations are described in the literature [15,16].

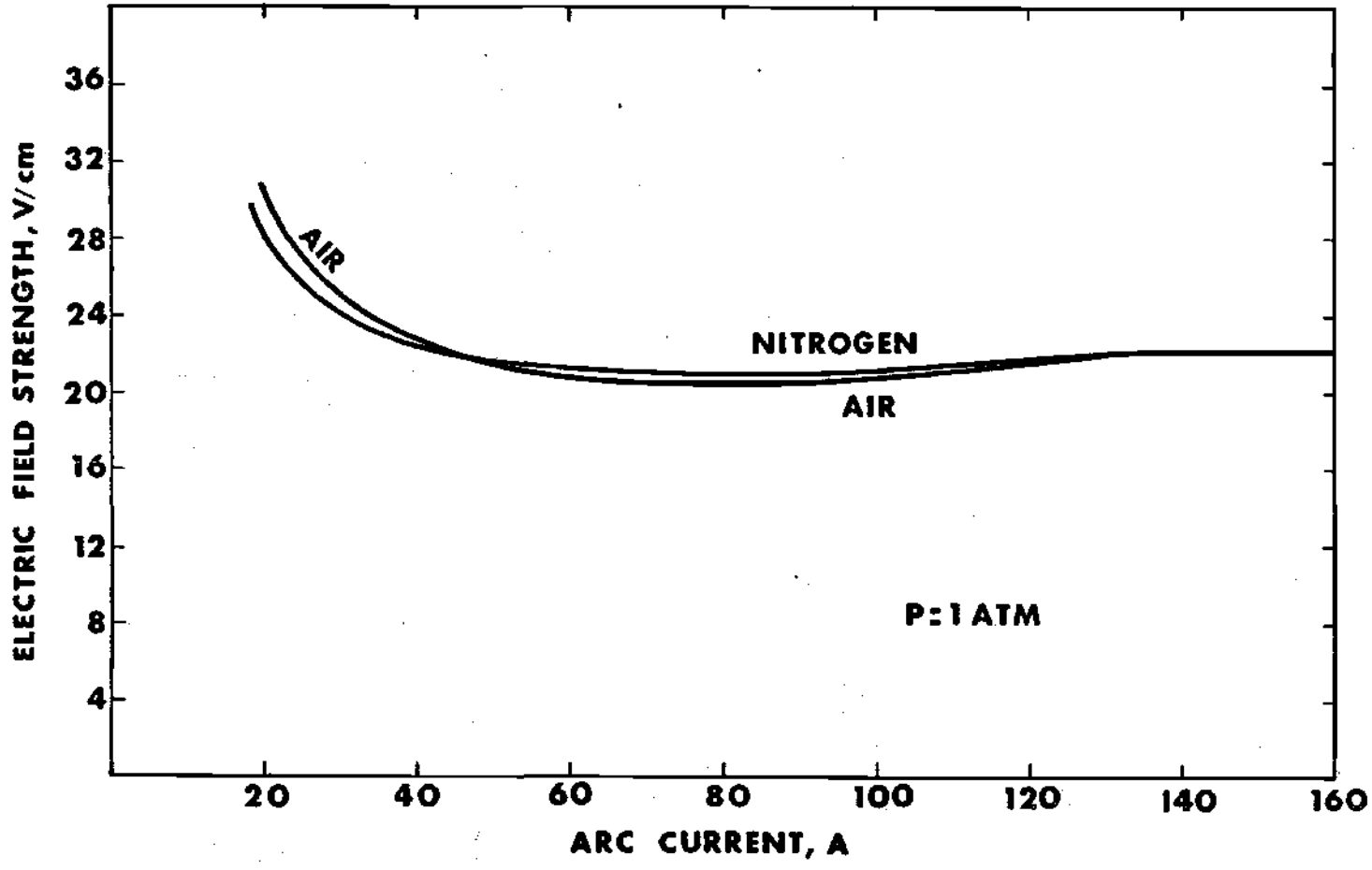

Figure 4. Electric Field Strength of Air Compared to Nitrogen

CHAPTER VI

POWER RADIATED PER UNIT ARC LENGTH FOR AIR

The power radiated per unit arc length was calculated from the thermopile data collected at various currents. In this reduction of data the following relation was used to determine the power radiated per unit length, P_R:

$$T_R = P_R \left(\frac{\omega}{4\pi}\right)(\ell')(\tau) \tag{6-1}$$

where:

ω = solid angle

ℓ' = apparent length of the arc, cm

τ = transmittance of quartz windows

T_R = thermopile reading, W

P_R = power radiated, W/cm

From this relation one may determine P_R as:

$$P_R = T_R \left(\frac{4\pi}{\omega}\right)\left(\frac{1}{\ell'}\right)\left(\frac{1}{\tau}\right) \tag{6-2}$$

The transmittance of the fused quartz windows was determined using the relation and method shown in Appendix B. This analysis assumed that the angle of incidence was approximately normal to the plane of the quartz plate, and

would not be changed significantly if the incident angle was as large as 30°.

The apparent length of the arc, ℓ', is a term used to designate the length of the plasma which would be intercepted by the thermopile if no light were blocked by the slit. As seen from Figure 10, there are two portions of the light intercepted by the thermopile element. One portion, the unshaded one, is the part in which every emitting particle in the plasma radiates energy to the entire area of the receiving element. The other portion, called the shaded region, is the part in which the emitting particles can only emit light to a portion of the thermopile. The rest of this light is blocked by the razor blade slit. The technique for determining this length assumes that the arc has a uniform emissive power. The length is determined by evaluating $\int\theta dA$ (shown in Figure 14) for the shaded region and setting it equal to the integral for the unshaded region. The apparent length can then be determined from these quantities. This method is described in more detail in Appendix A.

The solid angle, ω, was determined by assuming that the arc emitted most of its radiation at the axis. Therefore it was assumed that the plasma emitted as a line. The error involved in this assumption is quite small due to the distances involved. In fact, the angles involved in the calculation of the solid angle were, at most, one-tenth of a degree, of which the cosine is approximately one. Therefore

the solid angle may be determined on the basis of two differential elements with coincident normals. This formula is:

$$\omega = \frac{A_2}{S^2} \tag{6-3}$$

where:

A_2 = area of thermopile

S = distance between arc and thermopile

Appendix C presents, in greater detail, the various assumptions involved in arriving at this relation.

Using the method outlined above, the power radiated per unit length was calculated for a number of currents ranging from 28 amps to 140 amps. The results of these calculations are shown by the points indicated in Figure 5. A smooth curve was drawn through these points (also shown in Figure 5). This was done so that the calculation of the total radiation per unit volume could be done using a smooth and continuous function.

Noticeable scatter of data points was observed, mainly in the region below 40 amperes. This scatter can be attributed to the fact that the intensity of radiation from the arc was low compared with the background interference. In fact, attempts to measure the emitted radiation at currents lower than 28 amperes resulted in signals which were inseparable from the radiation of the surroundings. The

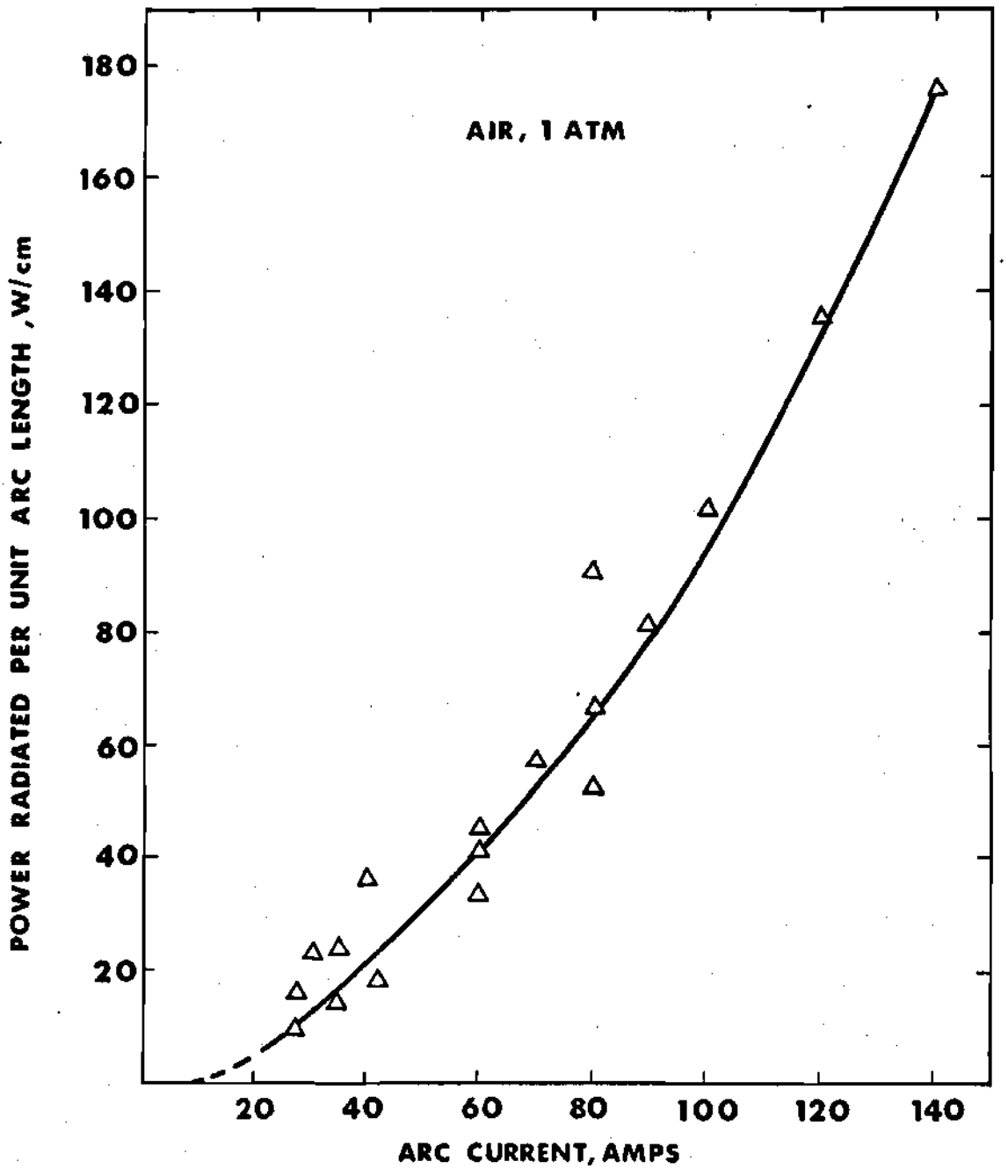

Figure 5. Power Radiated Per Unit Arc Length for Air

remaining points lie within approximately 20% of the curve values except for the upper data point calculated at 80 amps. This point deviates from the curve by about 45%, twice the divergence of the other points. There are two possible explanations for this deviation. One, there was an error made in measuring the radiation at that point; or, two, the power input to the arc was larger than recorded. The latter explanation is plausible because increasing the current to 90-100 amps would not be noticeable in the arc characteristic since this curve, Figure 3, is essentially flat in this region. However, the radiation increases sharply in this region.

Figures 6 and 7 are comparisons between the power radiated from nitrogen [14] and the power radiated from air. Figure 6 compares the radiative power of air and nitrogen on the basis of arc current. Figure 7, on the other hand, shows the comparison between nitrogen and air as a function of total power in the cascade. These two figures show roughly the same comparison due to the fact that the electric field strengths (Figure 4) are very similar for these two gases.

Values from this smoothed curve were used in the calculation of the total radiation emitted per unit volume. This topic is discussed in the next section.

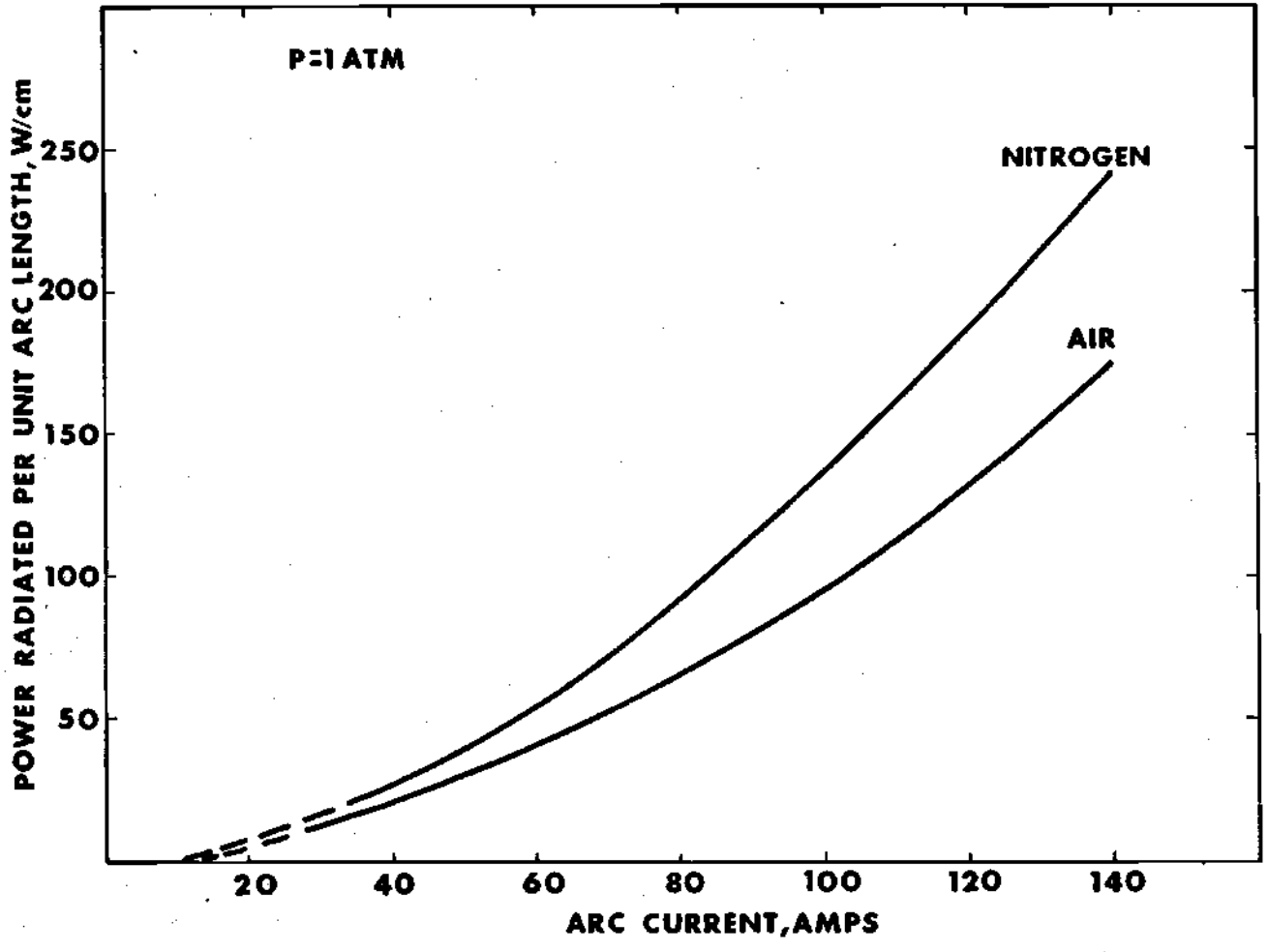

Figure 6. Power Radiated From Air and Nitrogen as a Function of Arc Current

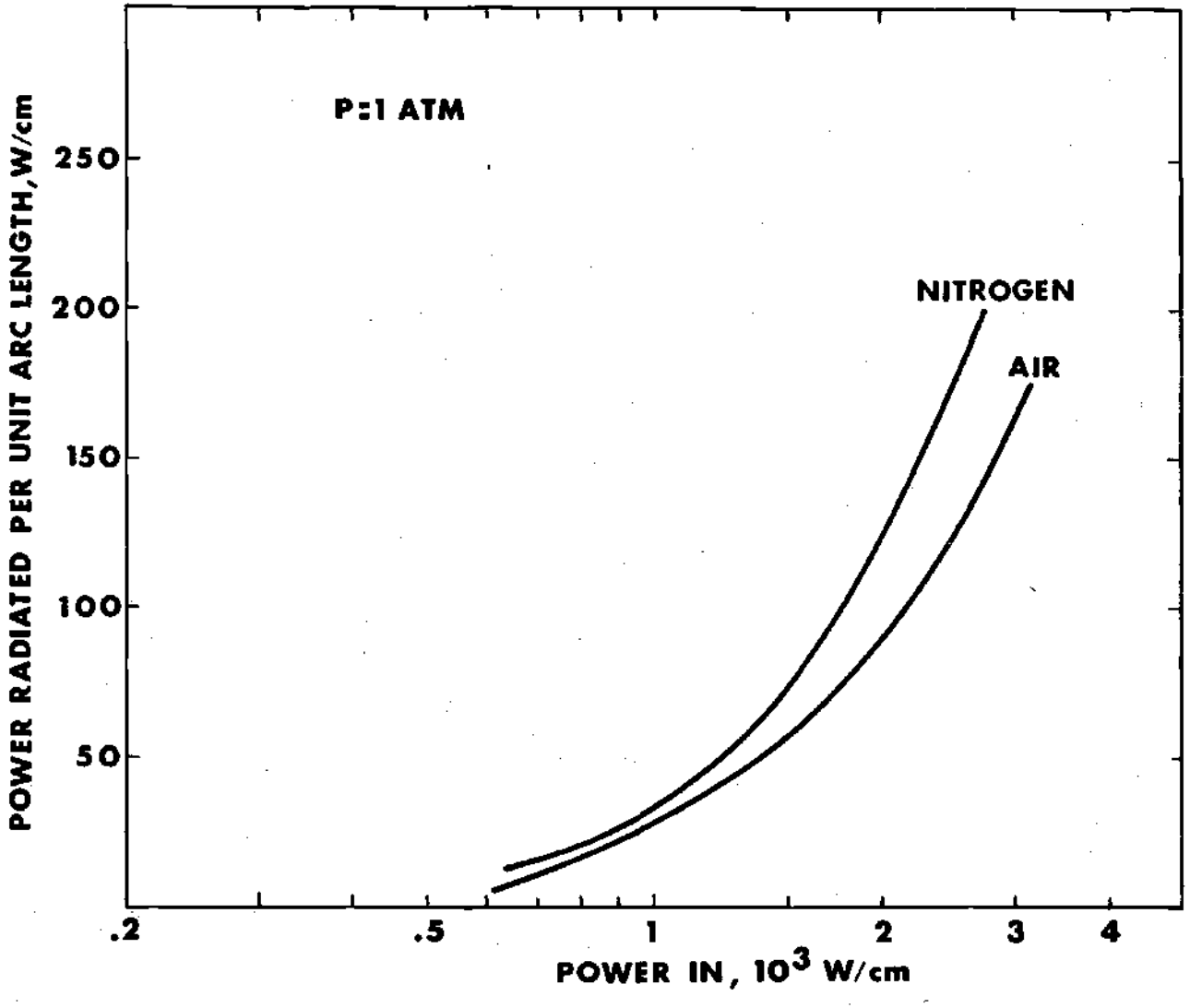

Figure 7. Power Radiated from Air and Nitrogen as a Function of Power In

CHAPTER VII

TOTAL RADIATION AS MEASURED FOR AIR

Determination of the total volumetric radiation coefficient, U(T), was achieved by solving the Volterra integral equation using a numerical technique described by G. Schmidt and H. Patt [15].

This Volterra integral equation can be written as follows [15]:

$$P_R(T_a) = \pi R^2 \int_{T_w}^{T_a} U(T) \frac{\partial}{\partial T} [-\rho^2(T,T_a)]dT \qquad (7\text{-}1)$$

where

P_R = power radiated/unit arc length, W/cm

T_a = axis temperature of the arc, °K

T_w = wall temperature, °K

R = radius of arc channel, 2.5 mm

$U(T)$ = total volumetric radiation coefficient, W/cm^3

ρ = normalized radius

This equation is obtained from the definition of the power radiated per unit arc length, P_R, which is:

$$P_R = \int_0^{\ell} \int_0^{2\pi} \int_0^{R} U(r) r dr d\phi dz \qquad (7\text{-}2)$$

which, in the case of cylindrical symmetry, reduces to:

$$P_R = 2\pi R^2 \int_0^1 U \rho d\rho \qquad (7\text{-}3)$$

Now, since the radial temperatures were known [5], a change in the variables of integration from normalized radius, ρ, to temperature, T, results in the Volterra integral equation stated above.

As formulated by G. Schmidt and H. Patt, the solution for obtaining U(T) can be written in terms of the axis temperature as follows:

$$U_k(T_a) = U(T_w) + \sum_{L=1}^{k} B_L \Delta T_L \qquad (7\text{-}4)$$

$$\text{for } k = 1, 2, 3, \ldots.$$

where:

ΔT_L = the difference in successive axis temperatures

$U(T_w)$ = the value of the total radiation evaluated at the wall temperature, T_w

B_L = slope of the total radiation curve between successive axis temperatures

The coefficient, B_L, which has units of W/cm^3 °K, was

determined from the power radiated per unit arc length and the radial temperature profiles shown in Figures 8 and 9. The formula used to calculate B_L can be written as follows:

$$B_L = \frac{1}{\int_{Ta_{L-1}}^{Ta_L} \rho^2(T,Ta_L)dT}\left[\frac{P_R(Ta_L)}{\pi R^2} - U(T_w) - \sum_{k=1}^{L-1} B_k \int_{Ta_{k-1}}^{Ta_k} \rho^2(T,Ta_L)dT\right] \quad (7\text{-}5)$$

where, $\int_{Ta_{k-1}}^{Ta_k} \rho^2(T,Ta_L)dT$ represents the area between successive axis temperatures under a plot of temperature versus normalized radius squared. By graphing the temperatures in this way, the resulting curves can be approximated by a series of straight lines as shown in Figure 10.

The term $U(T_w)$ was neglected in the calculation of B_L and $U(T_a)$ due to the low radiative power of air at temperatures less than 8000°K. In investigations of nitrogen plasmas, results from Hermann and Schade [12] indicate that near the wall only a small portion of the total energy transported is due to radiation. The assumption that $U(T_w)$ is negligible is also supported by the fact that the temperature at the wall was a maximum of approximately 1000°K because of the low temperature required to keep the cascade plates from melting.

Sample calculations of U(T) are presented in Appendix D. In these calculations, temperatures were taken from

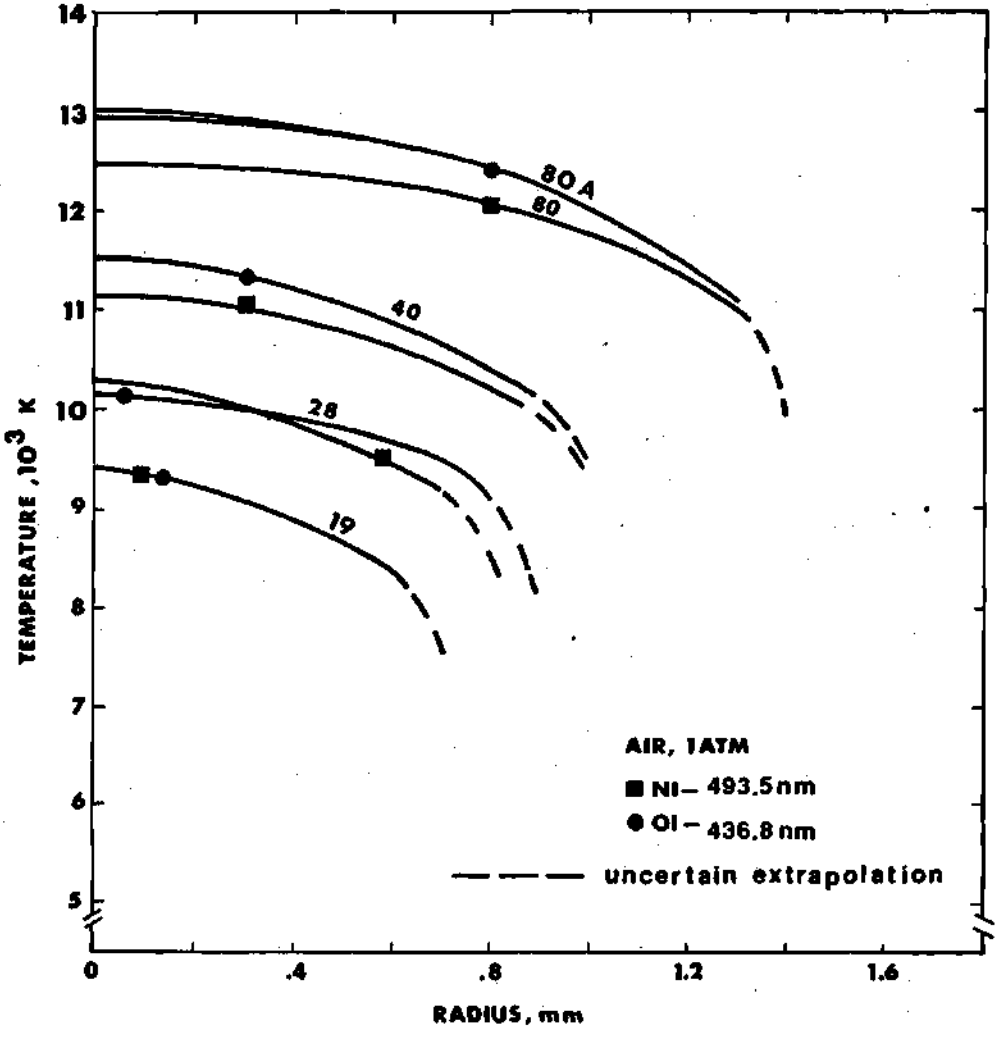

Figure 8. Radial Temperature Profiles Used for Calculating U(T)

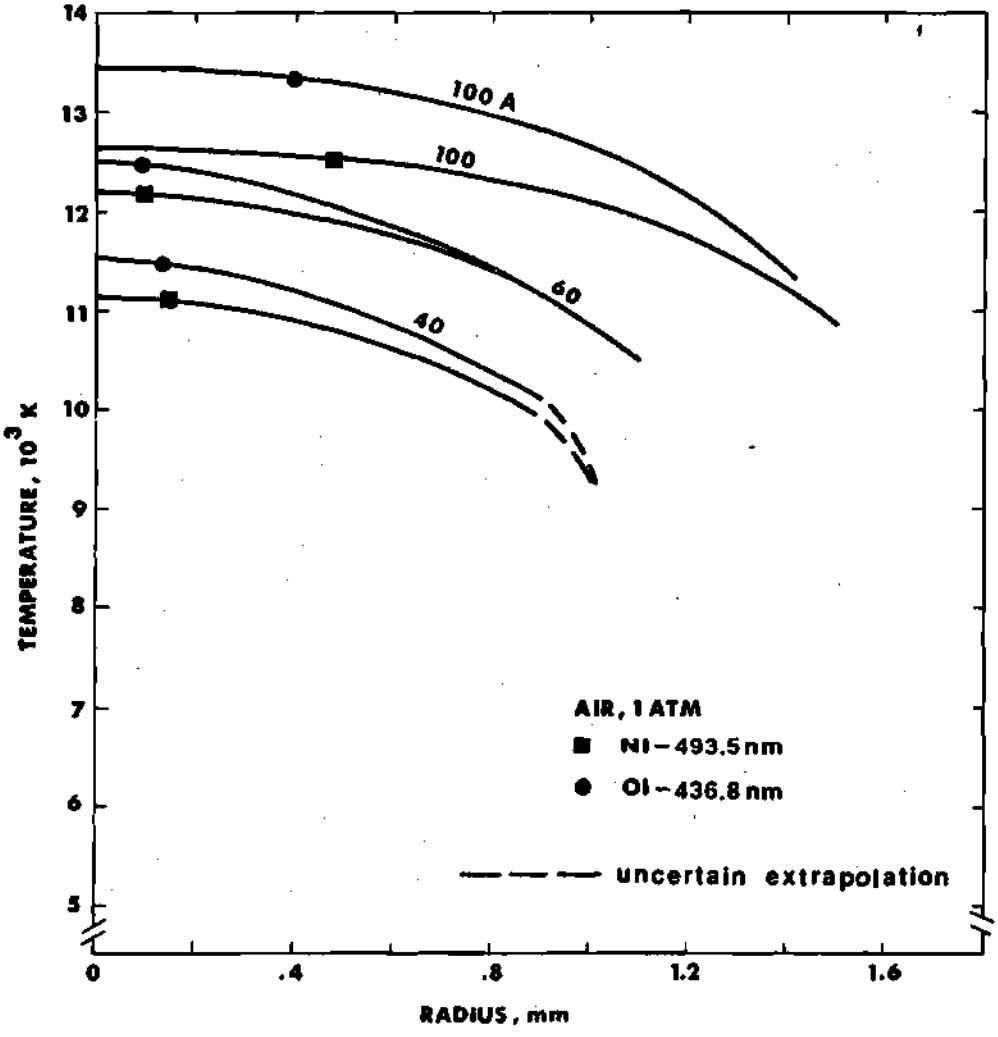

Figure 9. Radial Temperature Profiles Used for Calculating U(T)

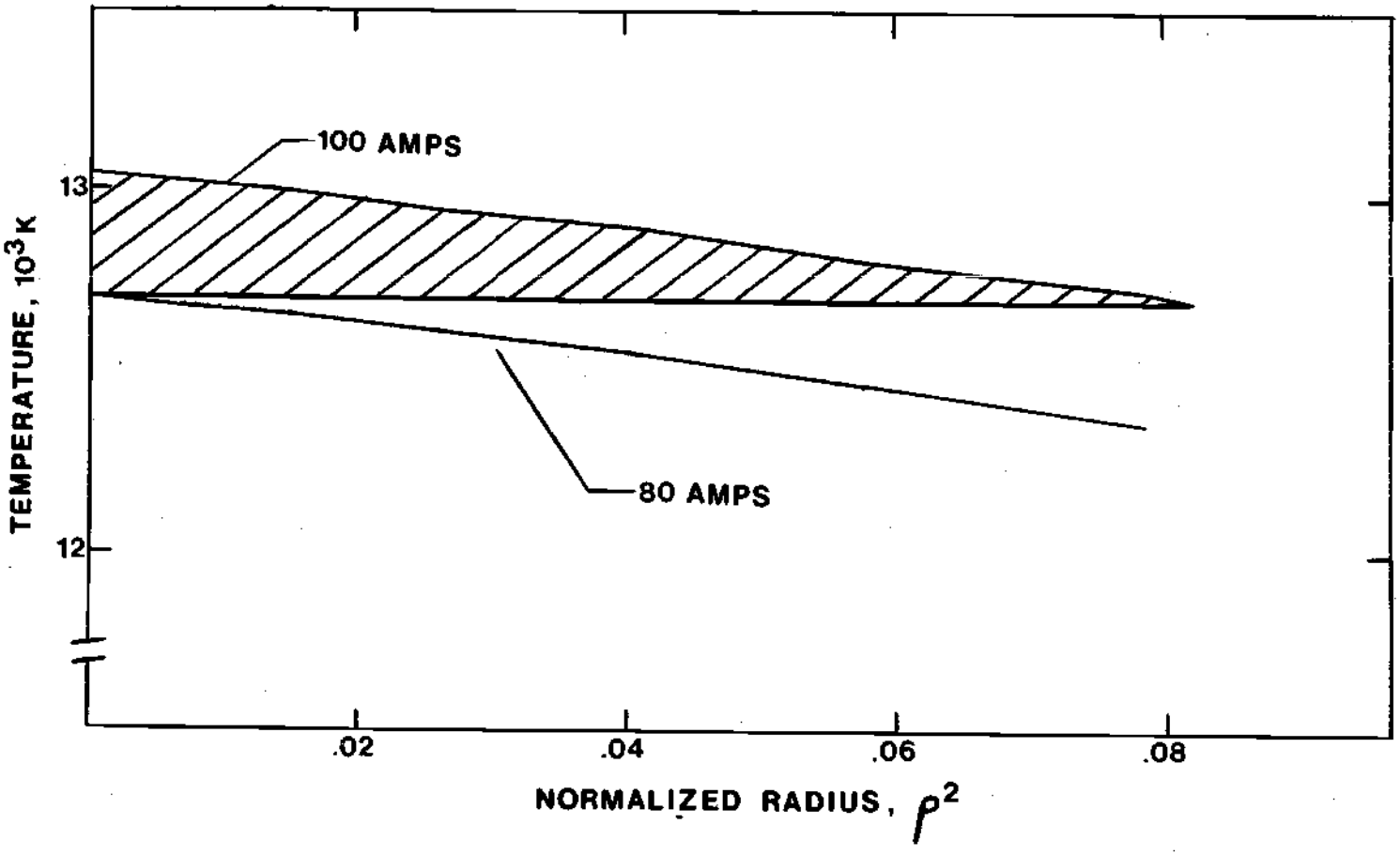

Figure 10. Temperature Versus Normalized Radius

average curves drawn from the oxygen and nitrogen temperature profiles shown in Figures 11 and 12.

Results of the calculations of total radiation emitted at the centerline temperature are shown in Figure 11. The points indicated on the drawing were calculated by the use of the numerical method explained above. From these points a smooth curve was drawn by using lines between these values as tangents to the function U(T).

Figure 12 is a comparative plot of the total radiation measured in this research, with the results in nitrogen from H. Maecker [14] and Asinovsky [4], and those of Schreiber [3] in air.

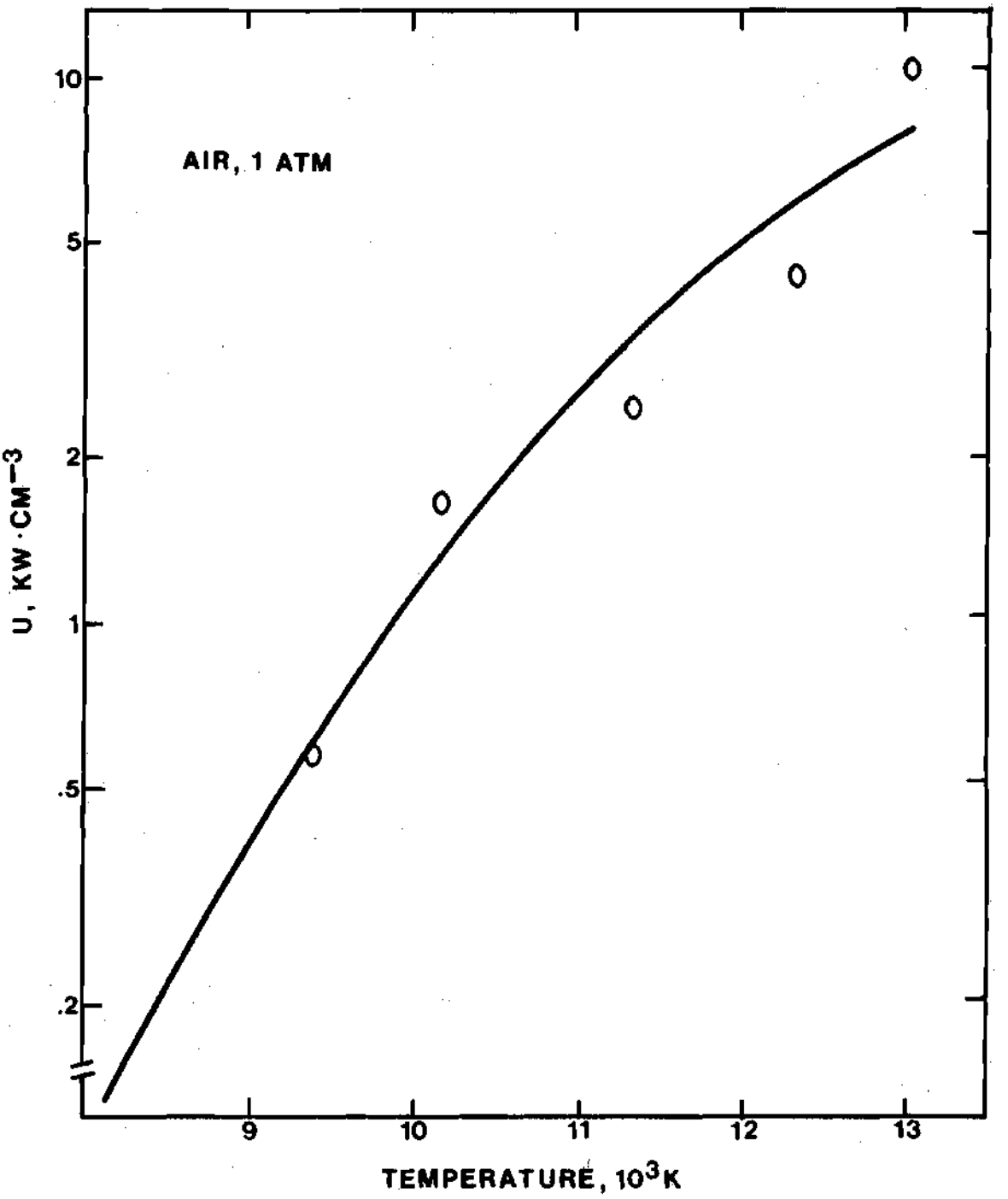

Figure 11. Total Radiation as Measured for Air (200 nm $\leq \lambda \leq$ 4000 nm)

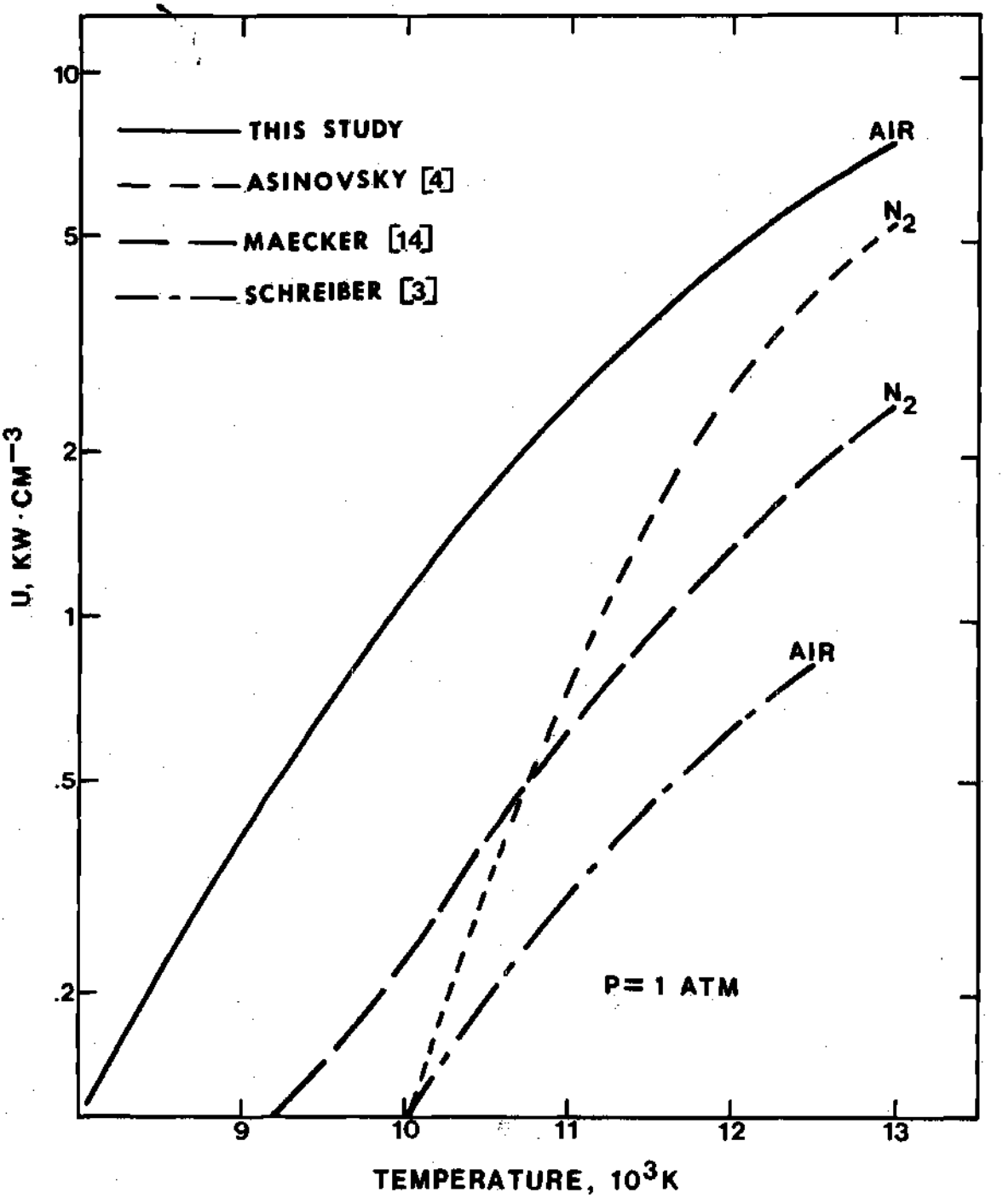

Figure 12. Total Radiation for Air and Nitrogen ($200\ nm \leq \lambda \leq 4000\ nm$)

CHAPTER VIII

CONCLUSIONS

Comparison of the measured field strengths in air at one atmosphere with the values obtained in an atmospheric nitrogen arc by Maecker [14] agreed closely. Reproducibility of this data, using the cascade plates as probes, was within the estimated error margin of $\pm$5%.

It was also determined that introducing air at low flow rates into the test section was possible at one atmosphere without noticeably disturbing the stability of the arc column or creating detectable convection effects. These conclusions were drawn from the flow, no-flow experiments described in Chapter IV.

Calculation of the total radiation of air at one atmosphere and comparison with results in nitrogen arcs from Maecker [14] and Asinovsky [4], and Schreiber's results in air [3] showed different degrees of deviation (Figure 12). The results of this study compared to within approximately 35% of Asinovsky's results for temperatures above 12,000°K, although this margin of difference was larger for lower temperatures. Both Maecker's results in nitrogen and Schreiber's results in air were consistently lower than the values obtained in this study. This difference may be due,

in part, to the numerical technique used in this research to calculate the total radiation. This explanation is substantiated by reports from other investigators [20,21], experiencing similar behavior of results after use of this particular numerical method.

The estimated error band present in these measurements is ±50%. This figure is the result of estimated error margins in the temperature profiles of ±10% and in the power radiated of ±20%. Also included in the estimation of the total error margin is the effect of the ±10% error in the temperature profiles on the area under a plot of temperature versus normalized radius squared (Figure 10). This error band was approximately ±20%.

Values of thermal and electrical conductivity will be calculated at a later date by other researchers. At the present time, however, attempts are being made to achieve stable operation with an air arc at pressures up to 30 atmospheres. Hopefully, operation at pressures of 250 atmospheres will be achieved, thus allowing measurements of the transport properties of air and application of these properties to high pressure air problems.

APPENDICES

APPENDIX A

CALCULATION OF TRANSMITTANCE

The ratio of reflected light to incident light is given by the relation [17]:

$$\phi = \left[\frac{n-1}{n+1}\right]^2 \qquad \text{(A-1)}$$

where:

n = index of refraction

ϕ = ratio of reflected light to incident light

Wien's displacement law was used at the average temperature obtained within the arc to determine the wavelength at which the maximum radiation is emitted (T = 12,000°K). At this temperature the following value of wavelength results:

$$\lambda_{max} = \frac{C_3}{T} = \frac{28978 \text{ (cm °K}}{12{,}000°K} \qquad \text{(A-2)}$$

$$\lambda_{max} = 241.5 \text{ nm}$$

At this value of wavelength the index of refraction is 1.51 [17]. Since there are four surfaces involved,

$$\tau = (1-\phi)^4 = .84 \qquad \text{(A-3)}$$

where τ is the fraction of light transmitted.

In this calculation the transmittance of the calcium fluoride window was not taken into account. It was assumed that the sensitivity of the thermopile, listed as 25 $\frac{\mu v}{\mu w}$, had the transmittance of the window incorporated into it. A correction of approximately .93 may be applied to the transmittance if the correction for the calcium fluoride is not assumed to be incorporated in the sensitivity.

APPENDIX B

CALCULATION OF THE APPARENT LENGTH

As shown in Figure 13, there are two areas which emit light received by the thermopile. The first is called the shaded area because the gas in this region emits light to only a certain portion of the thermopile. The portion of this light which would otherwise strike the thermopile is blocked out by the slit. The other portion of the area, called the unshaded region, emits light which is intercepted by the entire area of the thermopile.

For the shaded region the angle through which light is emitted may be formulated as follows (Figure 14):

$$\theta = \alpha - \beta \tag{B-1}$$

by the small angle approximation,

$$\alpha = \frac{y}{x}, \tag{B-2}$$

$$\beta = \frac{y-b}{x} \tag{B-3}$$

Therefore

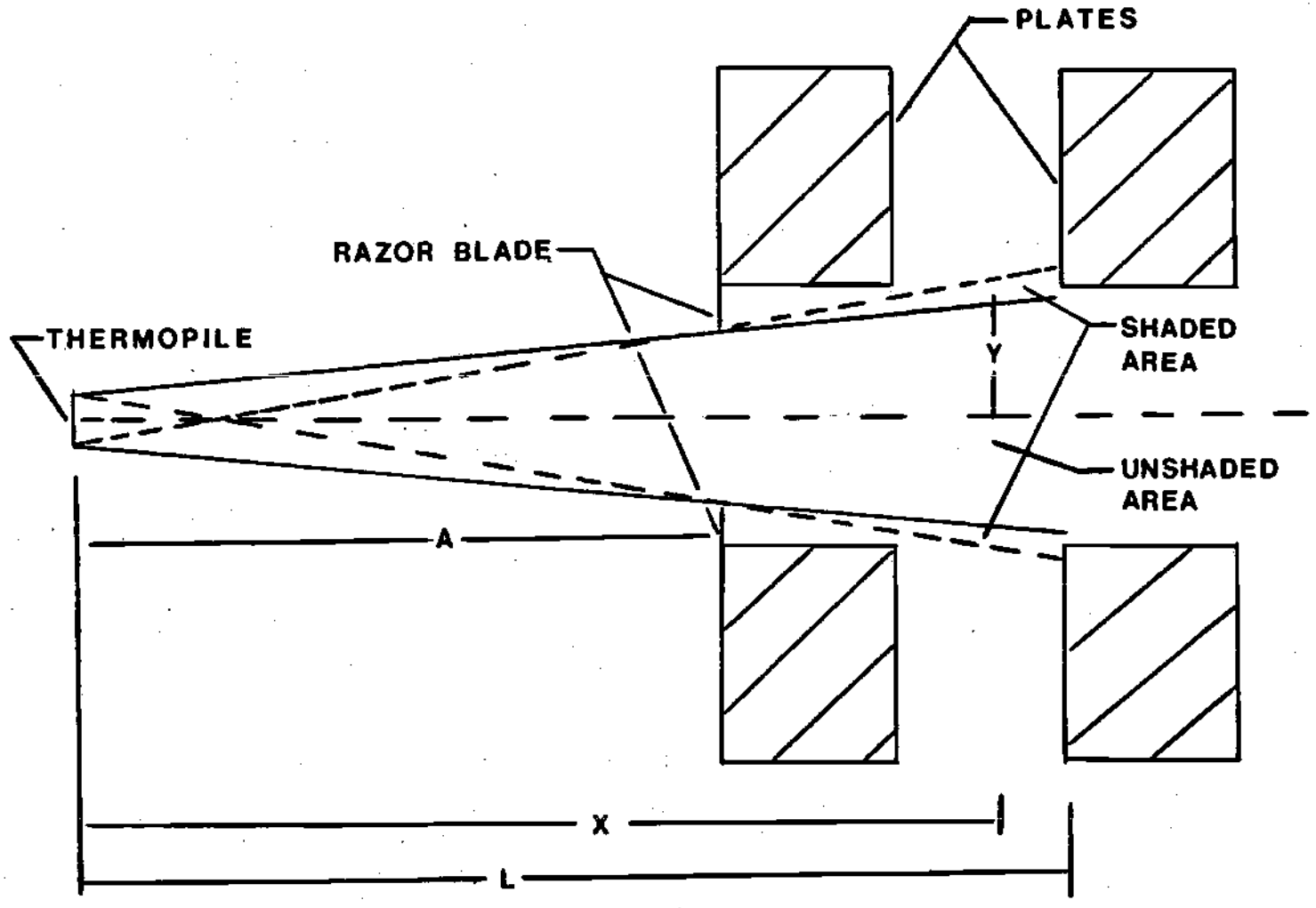

Figure 13. Schematic Diagram of Shaded and Unshaded Areas

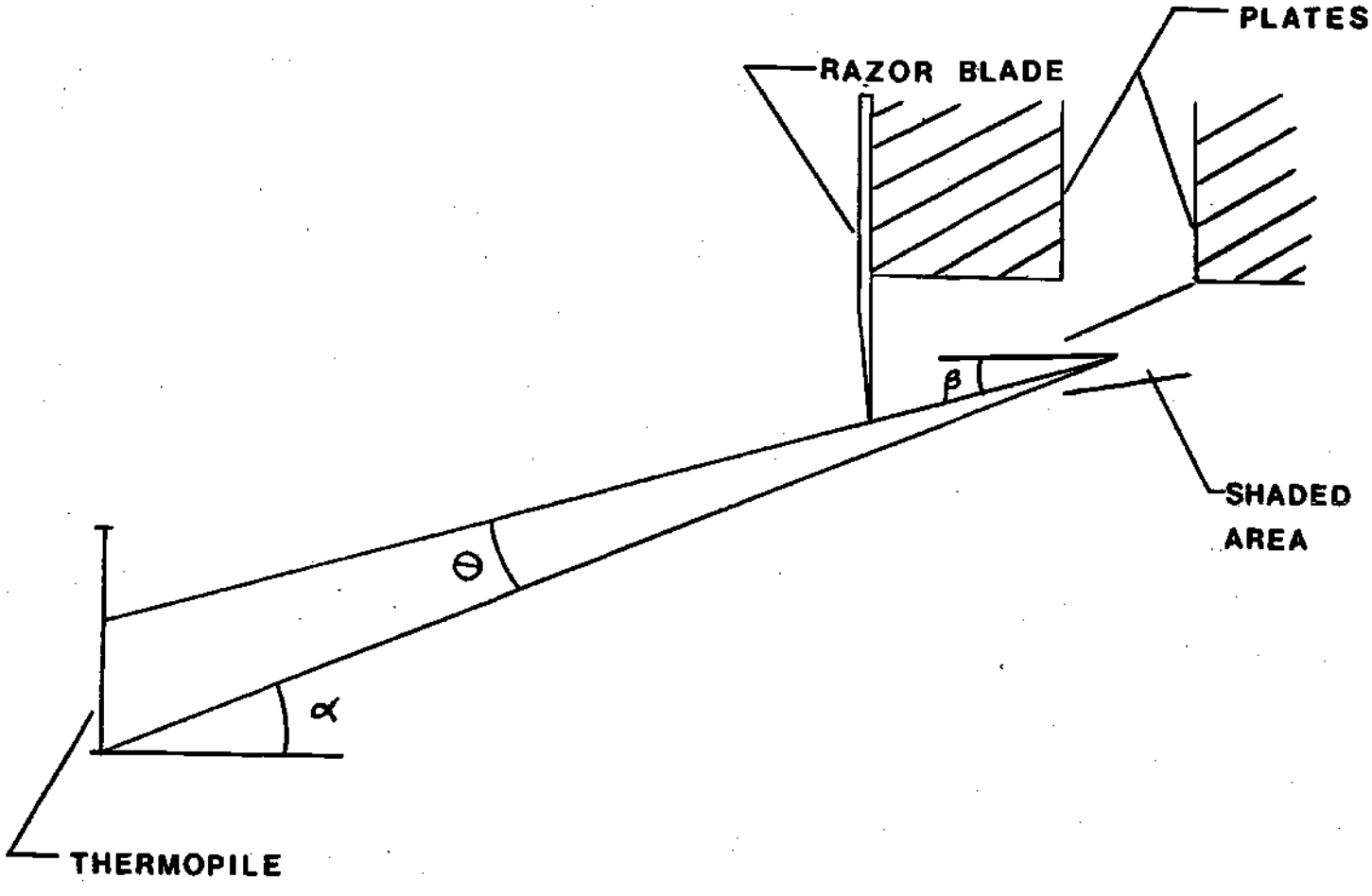

Figure 14. Angles Intercepted by Thermopile

$$\theta = \frac{b}{x} \tag{B-4}$$

Now, for the shaded region $\underline{b}$ may be written as

$$b = y - \frac{(y-.225)x}{(x-A)} \tag{B-5}$$

and

$$\theta = \frac{y}{x} - \frac{(y-.225)}{(x-A)} \tag{B-6}$$

To find the amount of area intercepted by the thermopile element, integrate over the area of the shaded portion as follows,

$$Z_s = \int_{x_o}^{x_1} \int_{y_o}^{y_1} \theta dA = \int_{x_o}^{x_1} \int_{y_o}^{y_1} \theta dxdy \tag{B-7}$$

Therefore,

$$Z_s = \int_{x_o}^{x_1} \int_{y_o}^{y_1} \left| \frac{y}{x} - \frac{(y-.225)}{(x-a)} \right| dydx \tag{B-8}$$

The limits on the vertical integration are the boundaries of the shaded areas. The horizontal integration is over the plasma diameter.

In the unshaded area, the total area of the element

receives radiation from each emitting particle.

Therefore in this case b = .2 (height of element) and,

$$\theta = \frac{.2}{x}$$

Integration of this function is performed by evaluating the following integral.

$$Z_{us} = \int_{x_o}^{x_1} \int_{d}^{y_o} \theta dA = \int_{x_o}^{x_1} \int_{d}^{y_o} (\frac{.2}{x}) dy dx \qquad \text{(B-9)}$$

where:

x_o and x_1 are the same as before

y_o is the upper limit of the unshaded area

d is a constant to be determined

To find the constant $\underline{d}$; Z_{us} is set equal to Z_s. Thus $\underline{d}$ may be determined.

When this has been done, the apparent length may be determined by the relation:

$$\ell' = 2[(w'-d) + w-.1] \qquad \text{(B-10)}$$

where:

$$w' = \left[\frac{.025}{a}\right](a + 28.15) + .1 \qquad \text{(B-11)}$$

$$w = \left[\frac{.025}{a}\right](a + 33.15) + .1 \qquad \text{(B-12)}$$

APPENDIX C

SOLID ANGLE CALCULATIONS

The arc is assumed to be emitting only from its axis. The basis for this is as follows:

(1) The axis is where the highest temperature is attained and therefore the radiative energy emitted is the greatest. Considering the energy transport as presented by Schade [11], the transport of energy decreases as the distance from the center of the arc increases.

(2) At the minimum distance of 46 cm used in these measurements, the cosine of the involved angles was approximately one.

Figure 11 illustrates the arrangement. Therefore, to determine the solid angle the analysis proceeds as follows.

From the definition of the shape factor [18]:

$$\frac{\cos\beta_1\cos\beta_2}{\pi S^2}\, dA_2 = \frac{\cos\beta_1}{\pi}\, d\omega \qquad \text{(C-1)}$$

integrating with respect to A_2 and ω results in:

$$\int_{A_2} \frac{\cos\beta_1\cos\beta_2}{\pi S^2}\, dA_2 = \int_{\omega} \frac{\cos\beta_1}{\pi}\, d\omega \qquad \text{(C-2)}$$

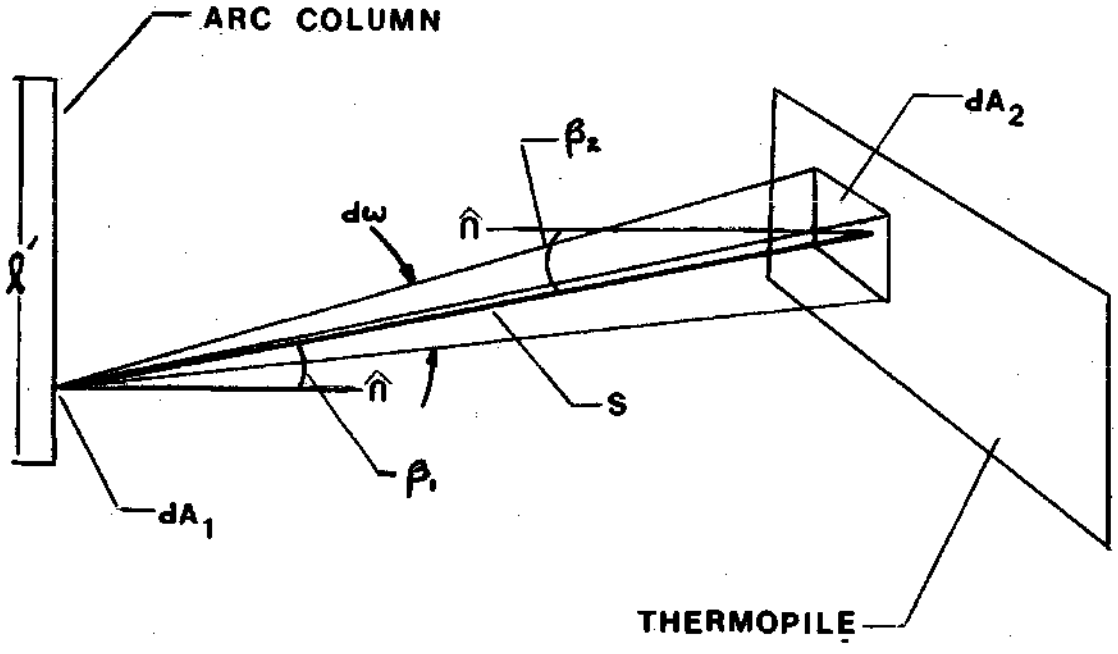

Figure 15. Solid Angle Intercepted by Thermopile

integration over A_1 is shown by:

$$\int_{A_1}\int_{A_2} \frac{\cos\beta_1\cos\beta_2}{\pi S^2}\, dA_2 = \int_{A}\int_{\omega} \frac{\cos\beta_1}{\pi}\, d\omega\, dA_1 \qquad (C\text{-}3)$$

In this case the area integral reduces to a line integral, since $A_1 = \ell'$.

Now these integrals can be rewritten as:

$$\int_{\ell'}\int_{A_2} \frac{\cos\beta_1\cos\beta_2}{\pi S^2}\, dA_2 d\ell' = \int_{\ell'}\int_{\omega} \frac{\cos\beta_1}{\pi}\, d\omega\, d\ell' \qquad (C\text{-}4)$$

Now using the assumptions that:

(1) $\cos\beta_1 = \cos\beta_2 \cong 1$

(2) S = constant

the result is as follows:

$$\frac{1}{\pi S^2}\int_{\ell'}\int_{A_2} dA_2 d\ell' = \frac{1}{\pi}\int_{\ell'}\int_{\omega} d\omega d\ell' \qquad (C\text{-}5)$$

$$\frac{A_2\ell'}{\pi S^2} = \frac{\omega\ell''}{\pi} \qquad (C\text{-}6)$$

Therefore:

$$\omega = \frac{A_2}{S^2} \qquad (C\text{-}7)$$

APPENDIX D

SAMPLE CALCULATIONS FOR U(T)

Calculation of the total radiation, U(T), using the numerical technique described by Schmidt and Patt [15] was performed as follows. First, the "B" coefficients were calculated from the following formula:

$$B_N = \frac{1}{\int_{Ta_{n-1}}^{Ta_n} \rho^2(T,Ta_n)dT} \left[\frac{P_R(Ta_n)}{\pi R^2} - U(T_w) - \sum_{k=1}^{n-1} B_k \int_{Ta_{k-1}}^{Ta_k} \rho^2(T,Ta_n)dT\right] \tag{7-5}$$

The total radiation emitted at the wall temperature, T_w, was neglected for the reasons stated in Chapter VII.

Several starting points were tried but the one which produced the smoothest curve was T_o = 7600°K. Using this starting point and the next higher axis temperature, T_1 = 9400°K, the area, between these temperatures, under a plot similar to the one shown in Figure 10 was determined. Therefore,

$$\int_{7600}^{9400} \rho^2(T,9400)dT = 78.4°K$$

The power radiated per unit length, P_R, was obtained from Figure 5 as,

$$P_R(9400) = 5 \text{ W/cm}$$

The first coefficient, B_1, was then calculated to be,

$$B_1 = \frac{(1)}{78.4 \text{ K}} \frac{(5 \text{ W/cm})}{(.25)^2} \text{cm}^2 = .325 \text{ W/cm}^3 \cdot \cdot \text{°K}$$

The next step was to determine U(9400) from the formula,

$$U_k(T_a) = \sum_{L=1}^{k} B_L \Delta T_L$$

Therefore, for a centerline temperature of 9400°K (k=1) the result is,

$$U_1(9400) = \sum_{L=1}^{1} B_L \Delta T_L = B_1(9400\text{-}7600)$$

$$U_1(9400) = (.325 \text{ W/cm}^3 \cdot \text{°K})(1800\text{°K}) = 585 \text{ W/cm}^3$$

This procedure was followed in calculating the total radiation emitted at the remaining centerline temperatures. These calculations resulted in the curve shown in Figure 11.

REFERENCES

1. J. M. Yos, Avco Technical Memorandum, RAD-TM-63-7, (revised, 1967).

2. U. H. Bauder and H. Maecker, Proceedings of IEEE, 59, 588 (1971).

3. P. Schreiber, A. M. Hunter, and K. R. Benedetoo, "Electrical Conductivity and Total Emission Coefficient of Air Plasma," AIAA Journal, 11, 815 (1973).

4. E. I. Asinovsky, A. Y. Kirillin, E. P. Pakahomov, and V. I. Shabashov, "Experimental Investigation of Transport Properties of Low Temperature Plasma by Means of Electric Arc," Proceedings of the IEEE, 59, 592 (1971).

5. E. A. Shires, M. S. Thesis, School of Mechanical Engineering, Georgia Institute of Technology, (1974).

6. W. Hermann and E. Schade, "Radiative Energy Balance in Cylindrical Nitrogen Arcs," Journal of Quantitative Spectroscopy and Radiative Transfer, 12, 1257 (1972).

7. J. C. Morris, R. P. Rudis, and J. M. Yos, "Measurements of Electrical and Thermal Conductivity of Hydrogen, Nitrogen, and Argon at High Temperatures," Physics of Fluids, 13, 608 (1970).

8. E. Shulz-Goulde, "The Continuous Emission of Argon in the Visible Spectral Range," Zeitschrift fur Physik, 230, 449 (1970).

9. L. M. Biberman and G. N. Norman, Journal of Quantitative Spectroscopy and Radiative Transfer, 3, 221 (1963).

10. M. Sherman, P. Jacobs, and J. Grey, "Analytical-Experimental Correlation of Radiation Loss from an Argon-Arcjet," Report No. 658, U. S. Air Force.

11. U. H. Bauder, "Radiation from High-Pressure Plasmas, Journal of Applied Physics, 39, No. 1, 148 (1968).

12. W. Hermann and E. Schade, "Transportfunktionen von Stickstoff bis 26000°K," Zeitschrift fur Physik, 171, 449 (1963).

13. U. H. Bauder and E. Stephens, "An Apparatus to Investigate Plasmas at Very High Pressure," Review of Scientific Instruments, 43, 1341 (1972).

14. H. Maecker, private communication.

15. G. Schmidt and H. Patt, "Dic Bestimmung von Materialfunktionen eines Stickstoffplasmas bei Atmospharendruck bis 15000°K," Zeitschrift fur Physik, 171, 449 (1963).

16. R. S. Devoto and D. Mukherjee, Journal of Plasma Physik, 9, 65 (1973).

17. Robert C. Weast, ed., Handbook of Chemistry and Physics, Chemical Rubber Co., Cleveland, Ohio, E-233 (1969).

18. Robert Siegel and John R. Howell, Thermal Radiation Heat Transfer, McGraw-Hill, New York, 176 (1972).

19. H. Maecker, Z. Naturforsch, 119, 457 (1956).

20. R. S. Devoto, private communication.

21. U. H. Bauder, private communication.